Supporting Information

Carrier mobility of two-dimensional Dirac materials: the influence from optical phonon scattering

Yingqi Wang[a], *Zijian Wang*[a], *Ting Cheng*[a,b] *and Zhirong Liu*[a,c*]

[a] College of Chemistry and Molecular Engineering, Peking University, Beijing 100871, China.

[b] Center for Nanochemistry, Academy for Advanced Interdisciplinary Studies, Peking University, Beijing 100871, China

[c] State Key Laboratory for Structural Chemistry of Unstable and Stable Species, Beijing National Laboratory for Molecular Sciences, Peking University, Beijing 100871, China

Sec. A. Optical deformation potential vs. gauge field

The (zeroth order) optical deformation potential is defined as the linear response of the on-site energy to the atomic displacement.[1] Considering the effect of the optical deformation potential in general, Eq. (34) needs to be modified as

$$\Delta \boldsymbol{H}_{\mathbf{k}}(\mathbf{q},\eta) = \begin{pmatrix} D & S_\eta \\ \text{c. c.} & D \end{pmatrix} \frac{\epsilon}{\sqrt{\hbar/2M_{\text{cell}}\omega_{\mathbf{q}}}}, \tag{S1}$$

where $D \propto \frac{\partial e_{\text{on}}}{\partial \epsilon}$ denotes optical deformation potential. Under the perturbation of an optical phonon mode, the Dirac point's energy will be lifted by $D\epsilon/\sqrt{\hbar/2M_{\text{cell}}\omega_{\mathbf{q}}}$. Using graphene as an example,

we vary the C-C bond length in the primitive cell and calculate the band dispersion near **K** to obtain the energy shift of Dirac point, as shown in Fig. S1.

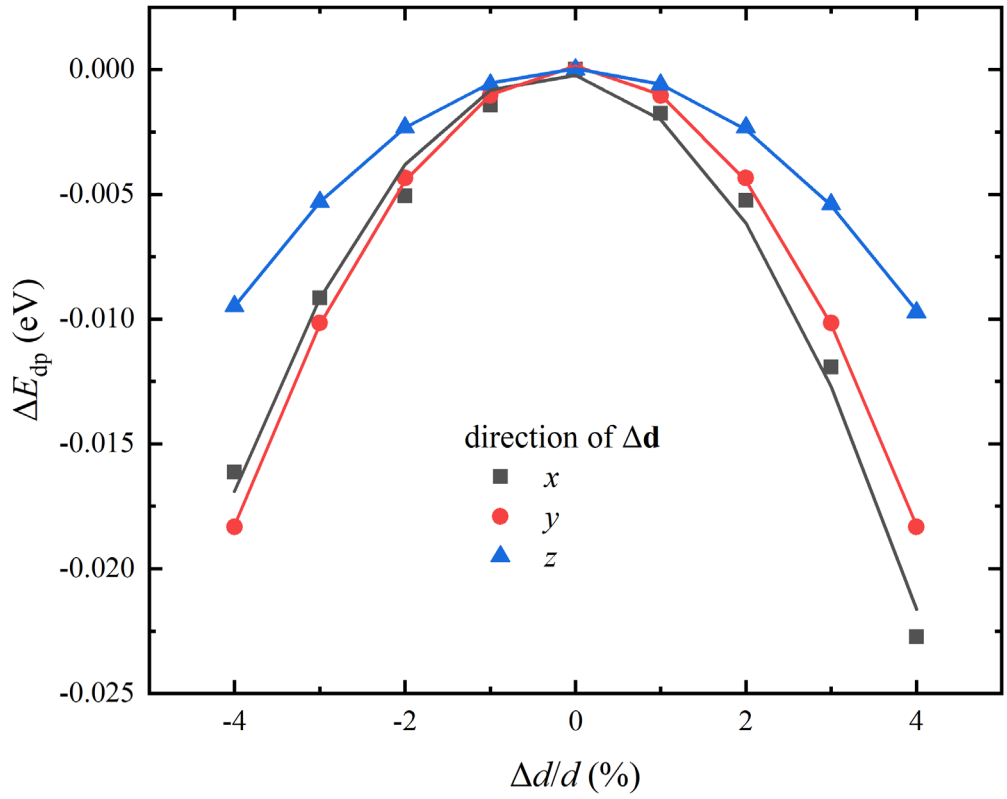

Figure S1. Variation of Dirac point energy. The horizontal coordinate is the percentage change in bond length. The energies of the Dirac point at different atomic displacements have been subtracted from their respective vacuum energy levels, making the ΔE_{dp} comparison valid.

The relationship between Dirac point energy change and bond length variation is in quadratic form, so the linear response of the e_{on} is zero. This is different from the case of the acoustic phonon, where both the deformation potential and the gauge field respond linearly to the strain tensor.[2] We further estimate the effect of the quadratic term, which is commonly referred to the coupling via the first-order interaction in deformation potential theory.[3] The average of Δd can be simply estimated from $\mu\omega^2\Delta d^2 = k_B T/2$, where μ is the effective mass $M_{\mathrm{C}}/2$. At $T = 300$ K, $\Delta d = 0.016$ Å, $\Delta d/d = 1\%$, $\Delta E_{\mathrm{dp}} = 0.001\sim0.002$ eV. Under the same Δd, the change of hopping

integral becomes $E_h \Delta d/\sqrt{\hbar/4M_C\omega_{\mathbf{q}}} = 0.22$ eV $\gg \Delta E_{\mathrm{dp}}$. Therefore, we prove that the effect of optical phonons on Δe_{on} is negligible. Note that for typical semiconductors the first-order deformation potential cannot be neglected, see Fig. S2.

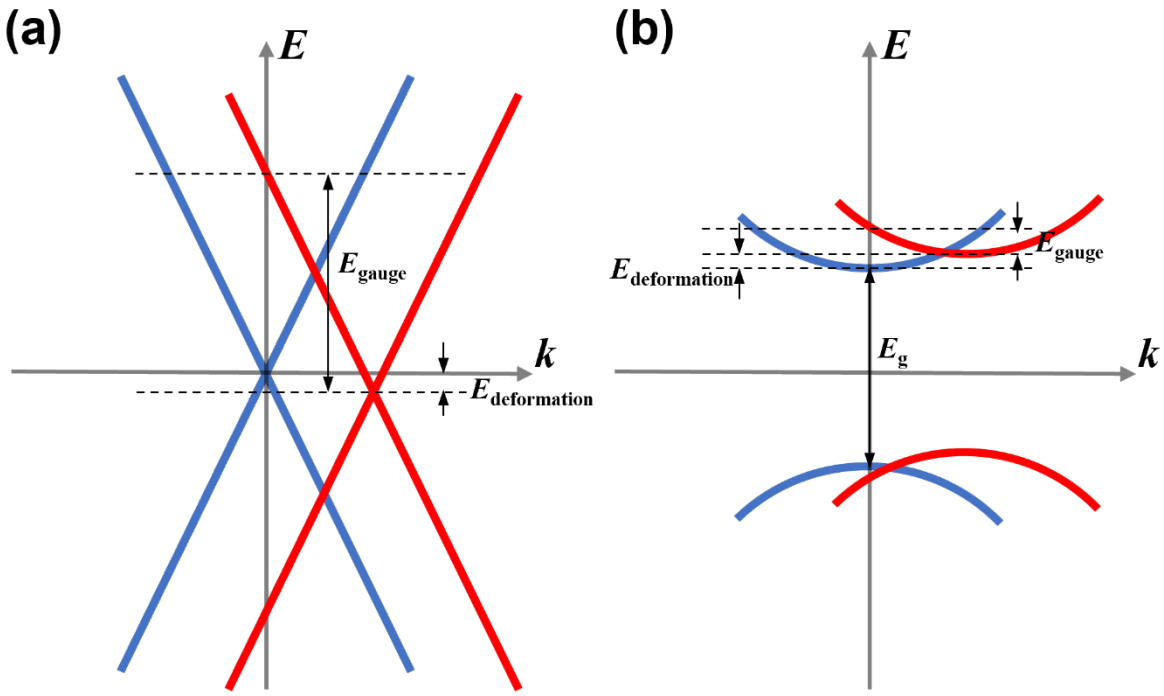

Figure S2. Schematic illustration of the effect of deformation potential and gauge field in (a) Dirac cones and (b) semiconductors. The blue and red lines represent the band structures before and after the atomic shift under optical phonon mode. The linear band dispersion of Dirac cone leads to the dominance of the gauge field.

Sec. B. Properties of VCl_3 monolayer

The density of states of VCl_3 monolayer is shown in Fig. S3. The density of states of spin-up and spin-down electrons are different. Near the Fermi energy, only spin-up electron states occur, these electronic states are mainly contributed by d_{xy} and $d_{x^2-y^2}$ orbitals of the V atom, with a small contribution from d_{yz} and d_{xz} orbitals, while spin-down electronic states present a huge

energy gap ($\Delta \approx 6$ eV). Only one spin channel contributes to the electron transport ($g = 2$ instead of 4 in graphene and α-graphyne).

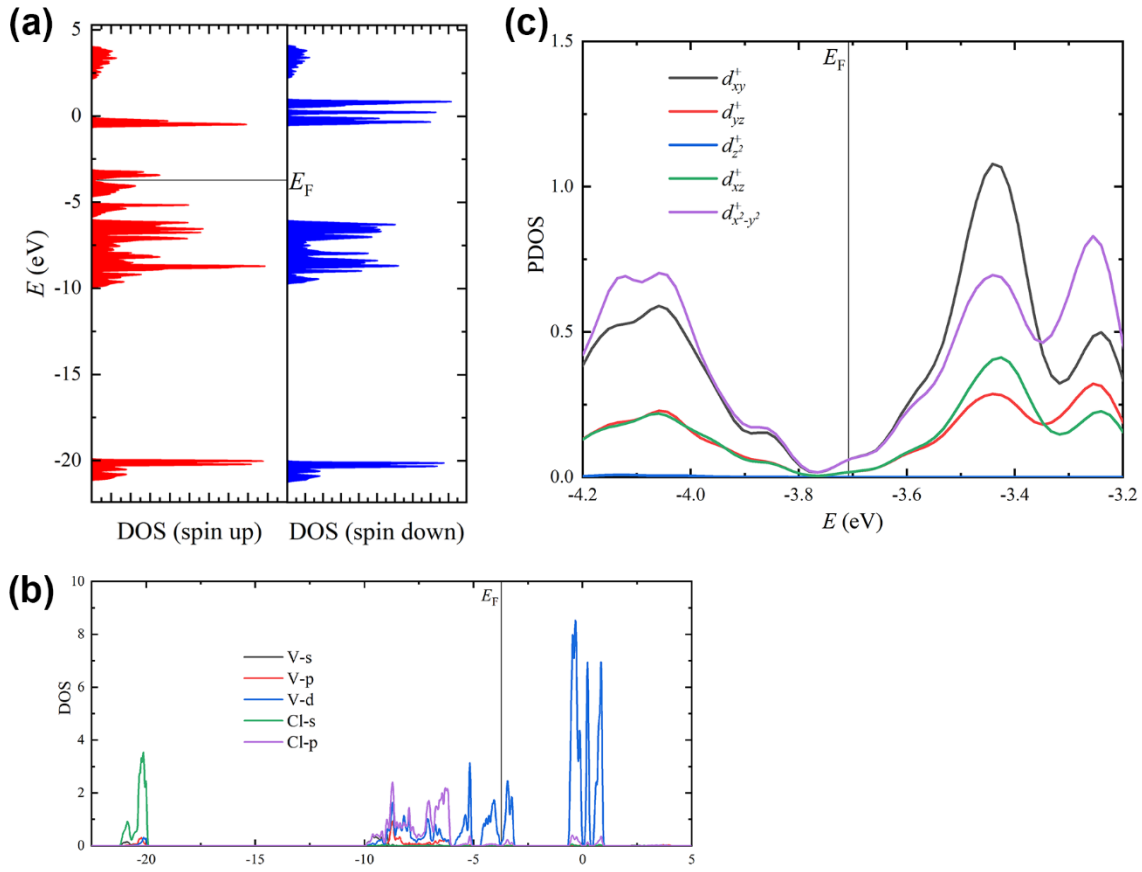

Figure S3. (a) total, (b) *l*-resolved (spin up) and (c) *lm*-resolved (spin up) DOS of VCl_3 monolayer. The unit of DOS is states/eV.

The parameters required to calculate the acoustic phonon limited mobility (Table 1) according to the generalized deformation potential theory proposed by Li et al.[2] are shown in Fig. S4. The elastic constants $C_{11} = 28.8\ \mathrm{J \cdot m^{-2}}, C_{44} = 9.76\ \mathrm{J \cdot m^{-2}}$ can be extracted directly from the phonon calculations. Li et al.[4] showed that when the system has in-plane C_3 symmetry, the pseudo-energy gap versus uniaxial/shear strain satisfies $\frac{\partial E_{\mathrm{gap}}}{\partial \epsilon(\mathrm{armchair})} = \frac{\partial E_{\mathrm{gap}}}{\partial \epsilon(\mathrm{zigzag})} = \frac{\partial E_{\mathrm{gap}}}{\partial \gamma}$ under the tight-binding approximation. Our simulation results confirm this property.

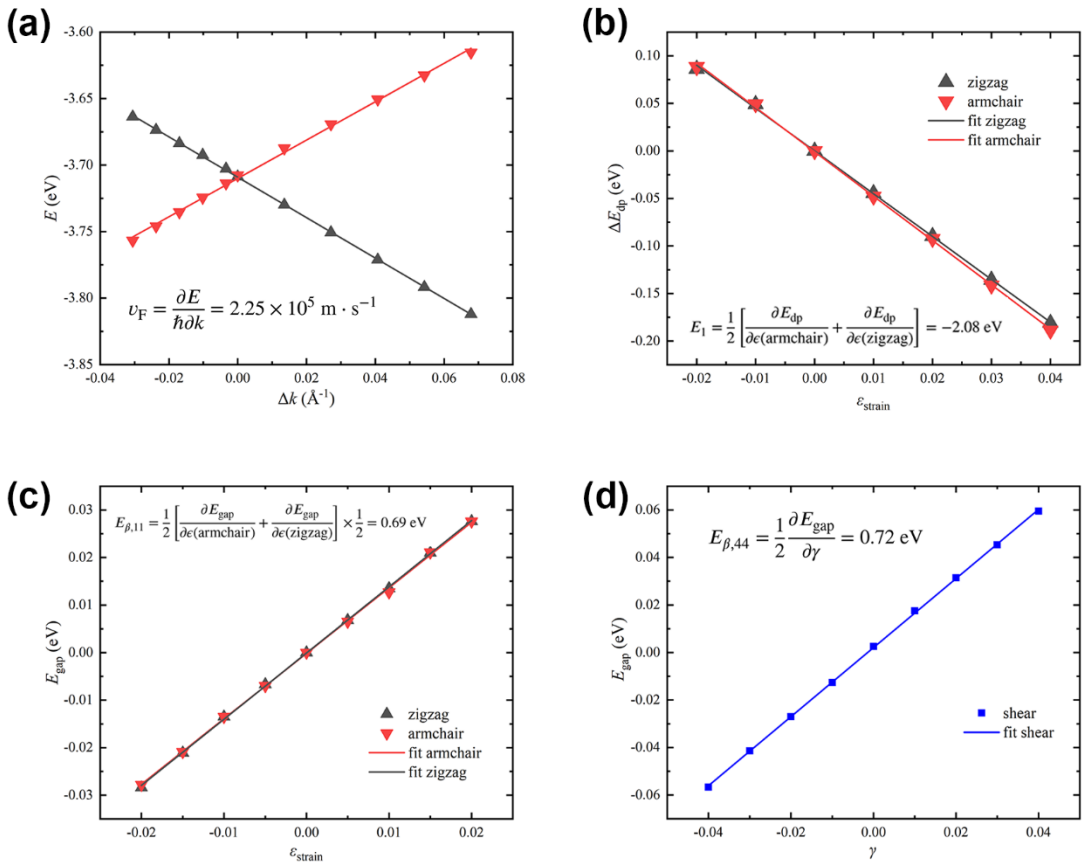

Figure S4. (a) Fermi velocity, (b) deformation potential constant, deformation hopping constant under (c) uniaxial, and (d) shear strain of VCl_3 monolayer.

More computational details of optical phonon limited mobility of VCl_3 monolayer are shown in Table S1. This corresponds to step 4 in the calculating process.

Table S1. The raw data for the calculation of $E_{h,\eta}$ in VCl_3 monolayer.

mode	frequency at **Γ** (cm^{-1})	degeneracy	$E_{pseudogap}$ ($\epsilon = 0.01$ Å)	$E_{pseudogap}$ ($\epsilon = 0.1$ Å)[a]	Relative displacement of V atoms[b]	$E_{h,\eta}$ (meV)
1	347.42	1	0.0000	0.0000	0	0
2	294.28	2	0.0094	0.0948	0.96 $\hat{\mathbf{y}}$	17.7
3	294.28	2	0.0094	0.0957	-0.96 $\hat{\mathbf{x}}$	17.7
4	273.54	1	0.0000	0.0000	0.84 $\hat{\mathbf{z}}$	0
5	273.50	2	0.0002	0.0062	0	1.2
6	273.50	2	0.0002	0.0062	0	1.2
7	273.18	1	0.0000	0.0001	0	0
8[c]	259.10	1	0.0016	0.0151	0	?
9	215.90	2	0.0000	0.0076	0	0
10	215.90	2	0.0000	0.0076	0	0

11	210.50	2	0.0030	0.0320	-0.10 $\hat{\mathbf{x}}$	7.4
12	210.50	2	0.0030	0.0305	0.10 $\hat{\mathbf{y}}$	7.4
13[d]	169.51	2	0.0001	0.0092	-1.02 $\hat{\mathbf{y}}$	0.2
14[d]	169.51	2	0.0001	0.0128	-1.02 $\hat{\mathbf{x}}$	0.2
15	145.39	2	0.0000	0.0054	0	0
16	145.39	2	0.0000	0.0054	0	0
17	144.68	1	0.0000	0.0000	1.03 $\hat{\mathbf{z}}$	0
18	117.12	1	0.0000	0.0000	0	0
19	95.18	1	0.0000	0.0000	0	0
20	89.58	2	0.0007	0.0093	-0.15 $\hat{\mathbf{x}}$	3.0
21	89.58	2	0.0007	0.0074	-0.15 $\hat{\mathbf{y}}$	3.0
22	0.00		0.0000	0.0001	0	
23	0.00		0.0000	0.0000	0	
24	0.00		0.0000	0.0000	0	

[a] $\epsilon = 0.1$ Å may be too large for calculating $E_{h,\eta}$. Some side effects may occur, like anharmonic effect, and the contribution of optical deformation potential. Normally at $T = 300$ K, according to the same approach in sec. A, the average displacement $\epsilon = 0.01\sim0.03$ Å, so we can safely adopt the pseudogap at $\epsilon = 0.01$ Å and ignore the optical deformation potential like graphene.

[b] The difference between the polarization vectors of the two V atoms in the unit cell.

[c] This mode needs further consideration, because the group theory analysis and tight-binding approach[5] do not predict an energy gap. (A real gap, not pseudogap)

[d] These modes present relatively large displacement of V atoms, but $E_{h,\eta}$ are very small.

Sec. C. More analyses of $\boldsymbol{\tau(k)}$, $\boldsymbol{F(\lambda)}$ and $\boldsymbol{F(\lambda,\beta\mu_0)}$

In this section, we will analyze the relaxation time equation [Eq. (19)], the integral $F(\lambda)$ [Eq. (26)] and $F(\lambda,\beta\mu_0)$ [Eq. (31)] in the main text in more detail and create an intuitive impression. According to Eq. (19), the relaxation time for electron scattering by optical phonons in Dirac materials is shown in Fig. S5(a). The "ghost-like" curve has three maximums located at $\epsilon(k) = 0$ and $\pm\hbar\omega_0$, and the height of "hands" is about twice the height of the "head" in linear scale.

We provide Table S2 to facilitate the calculation of $F(\lambda)$ by using the interpolation method. Perhaps a faster way to estimate $F(\lambda)$ is $\lg F \approx 1.65\lg\lambda - 0.56\lambda + 0.62\lambda\lg\lambda$. The maximum error for this approximation is about 15% [Fig. S5(b)]. For the case of charge doping, we investigate the effect of doping concentration on mobility. The doping concentration determines chemical potential by $n = \frac{g}{2\pi(\beta\hbar v_{\mathrm{F}})^2}\left[-\mathrm{Li}_2\left(-\mathrm{e}^{\beta\mu_0}\right)\right]$. According to [Eq. (30)], for a given optical

phonon branch, the mobility is proportional to $-F(\lambda,\beta\mu_0)/\mathrm{Li}_2\left(-\mathrm{e}^{\beta\mu_0}\right)$. Fig. S6(a) illustrates the relationship of carrier mobility and chemical potential on graphene. The carrier mobility caused by optical phonons first slightly rises and then decreases. Fig. S6(b) plots the $-\frac{F(\lambda,\beta\mu_0)}{\mathrm{Li}_2\left(-\mathrm{e}^{\beta\mu_0}\right)}\sim\beta\mu_0$ curve under various λ and Fig. S6(c) shows the mobility with charge doping compared to the neutrality point. Numerical calculations indicate that when λ is small (≤ 2.7), the carrier mobility monotonically decreases with $\beta\mu_0$, and when λ is large (≥ 2.7), the carrier mobility rises slightly then decreases with $\beta\mu_0$. One can also show that only for $\beta\mu_0 \gg \lambda$, i.e. the chemical potential is much larger than phonon energy, $\mu \propto n^{-1}$ holds (like acoustic phonon scattering).

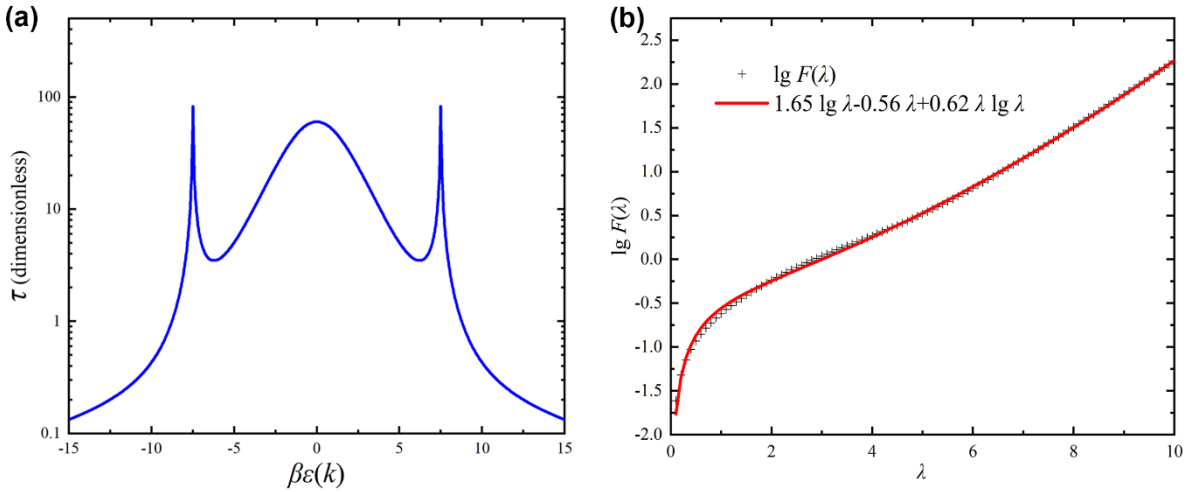

Figure S5. (a) Relaxation time of electron by optical phonon scattering. (b) $\lg F(\lambda)-\lambda$ relationship, and a fitting curve of $\lg F(\lambda)$.

Table S2 The relationship of $\lg F(\lambda)-\lambda$.

λ	$\lg F(\lambda)$	λ	$\lg F(\lambda)$	λ	$\lg F(\lambda)$	λ	$\lg F(\lambda)$	λ	$\lg F(\lambda)$
0.1	-1.61179	2.1	-0.20636	4.1	0.29163	6.1	0.84549	8.1	1.54512
0.2	-1.31833	2.2	-0.17641	4.2	0.31517	6.2	0.87795	8.2	1.58202
0.3	-1.14780	2.3	-0.14732	4.3	0.33900	6.3	0.91077	8.3	1.61903
0.4	-1.02655	2.4	-0.11906	4.4	0.36318	6.4	0.94394	8.4	1.65615
0.5	-0.93160	2.5	-0.09155	4.5	0.38775	6.5	0.97743	8.5	1.69338
0.6	-0.85279	2.6	-0.06476	4.6	0.41273	6.6	1.01122	8.6	1.73072

0.7	-0.78477	2.7	-0.03862	4.7	0.43816	6.7	1.04531	8.7	1.76815
0.8	-0.72438	2.8	-0.01309	4.8	0.46406	6.8	1.07967	8.8	1.80568
0.9	-0.66964	2.9	0.01190	4.9	0.49045	6.9	1.11428	8.9	1.84330
1.0	-0.61924	3.0	0.03640	5.0	0.51734	7.0	1.14914	9.0	1.88100
1.1	-0.57227	3.1	0.06047	5.1	0.54473	7.1	1.18423	9.1	1.91879
1.2	-0.52808	3.2	0.08418	5.2	0.57264	7.2	1.21953	9.2	1.95666
1.3	-0.48620	3.3	0.10758	5.3	0.60106	7.3	1.25503	9.3	1.99461
1.4	-0.44630	3.4	0.13075	5.4	0.62997	7.4	1.29073	9.4	2.03263
1.5	-0.40811	3.5	0.15374	5.5	0.65939	7.5	1.32660	9.5	2.07073
1.6	-0.37143	3.6	0.17662	5.6	0.68929	7.6	1.36265	9.6	2.10890
1.7	-0.33612	3.7	0.19946	5.7	0.71965	7.7	1.39885	9.7	2.14713
1.8	-0.30204	3.8	0.22232	5.8	0.75047	7.8	1.43521	9.8	2.18543
1.9	-0.26911	3.9	0.24526	5.9	0.78173	7.9	1.47171	9.9	2.22380
2.0	-0.23724	4.0	0.26835	6.0	0.81341	8.0	1.50835	10	2.26223

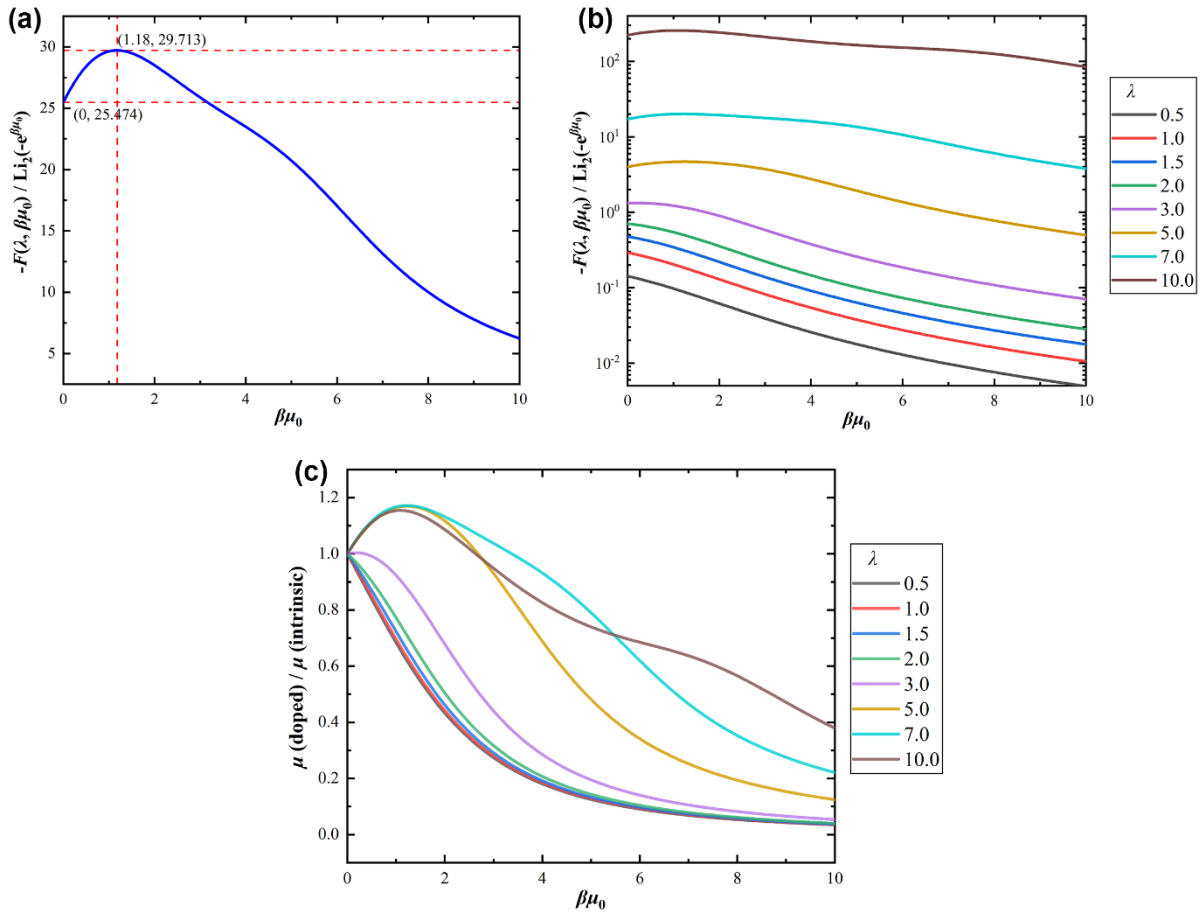

Figure S6. Properties of $F(\lambda, \beta\mu_0)$. (a) reflects the variation of graphene mobility (optical phonon limited, dimensionless) with doping concentration. (b) reflects the variation of mobility (dimensionless) with doping

concentration under various optical phonon frequency. (c) The comparison of mobility between doped and undoped case.

REFERENCES

1. Z. Li, P. Graziosi and N. Neophytou, *Phys. Rev. B*, 2021, **104**, 195201.
2. Z. Li, J. Wang and Z. Liu, *J. Chem. Phys.*, 2014, **141**, 144107.
3. K. Kaasbjerg, K. S. Thygesen and K. W. Jacobsen, *Phys. Rev. B*, 2012, **85**, 115317.
4. Z. Li, Z. Liu and Z. Liu, *Nano Res.*, 2017, **10**, 2005-2020.
5. H. Huang, W. Duan and Z. Liu, *New J. Phys.*, 2013, **15**, 023004.